AIAA JOURNAL
Vol. 33, No. 7, July 1995

Flow Structure on Stalled Delta Wing Subjected to Small Amplitude Pitching Oscillations

Kimberly M. Cipolla* and Donald Rockwell†
Lehigh University, Bethlehem, Pennsylvania 18015

The flow past a harmonically oscillating delta wing is investigated using high image-density particle image velocimetry. The overall objective is to alter the development of the leading-edge vortex and decrease the extent of stall on the wing. To this end, instantaneous velocity fields, contours of constant vorticity, and streamline patterns are obtained over an entire plane of the flow at successive instants of the wing motion. The degree of repeatability of the flow patterns during successive cycles of the wing oscillation is highly dependent on the dimensionless frequency of oscillation; it is possible to generate flow patterns that are phase locked at every cycle, as well as every other cycle, of the wing motion. In each case, a well-defined leading-edge vortex appears, and the instantaneous extent of the stall region is decreased relative to that on a stationary wing at the same angle of attack. However, cycle-averaged patterns show only minor departures from the flow structure on the stationary wing. Ensemble-averaged patterns, obtained by phase referencing to the wing motion, reveal that small-scale vortical structures originating in the unstable leading-edge shear layer are averaged out; the overall vorticity levels of the entire flowfield are lowered substantially, even for the average of only a small number of instantaneous images.

I. Introduction

THE unsteady aerodynamics of delta wings at high angle of attack has been the subject of many investigations in recent years, as aircraft supermaneuverability has become a priority. The flow structure is dominated by large-scale vortices formed from the leading edge of the wing. The existence of these vortices allows relatively high lift to be attained at high angle of attack. However, at sufficiently high angle of attack, there is breakdown of the leading-edge vortex. A further increase in angle of attack causes the vortex breakdown position to move upstream to the apex, and the separated flow to extend over the entire surface of the wing.

Unsteady, controlled motion of wings at long time scales (i.e., low pitch rates and low reduced frequencies) over large ranges of angle of attack has been studied, with the intent of altering the structure of the leading-edge vortex and the extent of stall. The wide variety of investigations in this category are summarized by Gad-el-Hak,[1] Magness et al.,[2] Lee and Ho,[3] Ashley et al.,[4] and Rockwell.[5] The principal features of this type of control are very substantial phase shifts between the wing motion and the location of vortex breakdown. Moreover, the cross-sectional development (with time) of the leading-edge vortex exhibits a substantial lag.

Controlled motion of the wing at shorter time scales and smaller variations of angle of attack has received considerably less attention. Imparting oscillations at a time scale on the order of the convective time scale c/U may allow manipulation of the unsteady leading-edge vortex and the degree of stall. There are certain equivalencies between unsteady motion of a wing in a steady stream and an unsteady stream past a stationary wing. Gursul et al.[6] showed that streamwise perturbations of the flow past delta wings could substantially alter the lift. Depending on the aspect ratio of the delta wing, phase-averaged lift coefficients up to 2.8 could be generated. The corresponding time-averaged lift coefficients were as high as 1.8. They conclude, using vorticity balance concepts, that convection of the leading-edge vorticity plays a central role in this lift enhancement.

The foregoing observations suggest that analogous, harmonic oscillations of a delta wing in a disturbance-free stream could have a significant effect on lift. The goal of the present investigation is to determine the classes of flow structure generated by such oscillations of a delta wing. Particle image velocimetry (PIV) is used to obtain two-dimensional velocity fields over an entire sectional plane of the flow. This approach allows comparison of instantaneous velocity fields with traditional representations involving cycle- and ensemble-averaged images and facilitates construction of the corresponding distributions of vorticity and patterns of streamlines. The effect of oscillation frequency and angle of attack on these patterns is addressed.

Received Sept. 28, 1993; revision received Aug. 8, 1994; accepted for publication Sept. 16, 1994.

*Graduate Research Assistant, Department of Mechanical Engineering.
†Paul B. Reinhold Professor, Department of Mechanical Engineering. Member AIAA.

II. Experimental System and Techniques

A. Experimental Apparatus

Experiments for this study were performed in a horizontal, steady water channel constructed of optically transparent Plexiglas® with large inlet and exit holding tanks. The test section is approximately 1 m wide by 5 m long with a typical water depth of 53 cm. The flow speed was 15 cm/s, corresponding to a Reynolds number based on the root chord of the wing of approximately 22,000.

The basic experimental apparatus, described in more detail by Cipolla,[7] consists of a Plexiglas half-delta wing attached to a rotating disk. A plan view is shown in Fig. 1. The disk is mounted within a Plexiglas vertical plate (false wall) to hold it away from the boundaries of the water channel and to isolate the drive train for the wing motion. The region of interest for the experiment is a plane parallel to the centerline of the wing, indicated by the dashed line.

A detailed drawing of the flat, sharp leading-edge delta wing is shown in Fig. 2. The characteristic aspect ratio S, defined as b^2/A, where b is the span and A is the planform area, is 4.0. The primary dimensions are: sweep angle $\Lambda = 45$ deg, root chord $c_0 = 17.8$ cm, and thickness $t = 1.25$ cm.

Oscillation of the delta wing is achieved via a Compumotor system that drives a gear attached to the rotating disk. Commands that define the wing motion are input to the laboratory microcomputer, converted into pulsed signals by an indexer, and sent to the motor driver to characterize the position, velocity, and acceleration of the wing. Since the time step between each Compumotor signal is 8 ms, which is two orders of magnitude smaller than the period of oscillation, smooth motion of the wing is ensured. An idler gear in the motor chain assembly promotes continuous transitions between clockwise and counter-clockwise rotations. The motor driver produces the appropriate current levels to actuate the Compumotor and, thereby, rotate the disk that holds the wing.

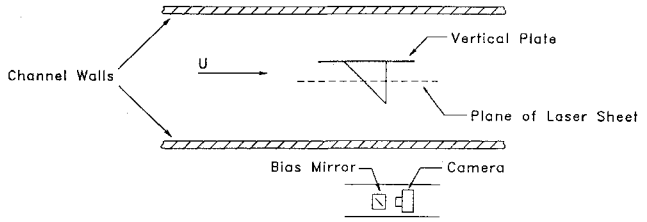

Fig. 1 Plan view of experimental system.

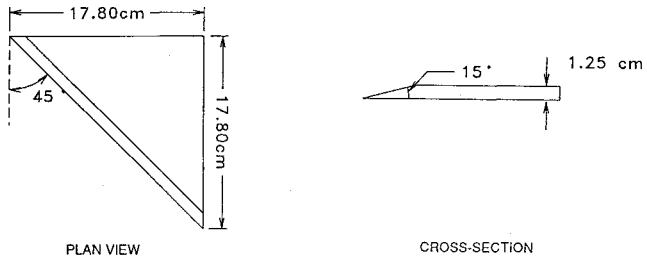

Fig. 2 Schematic of delta wing and its dimensions.

B. Experimental Techniques

Scanning particle image velocimetry was utilized in this experimental study to obtain instantaneous velocity distributions over an entire plane of the flow field. This approach is described by Rockwell et al.[8] A continuous, vertical laser sheet, approximately 1 mm in thickness, is generated by deflecting the laser beam from a multi- (72-) faceted rotating mirror. This laser sheet illuminates the seeding particles, which are 14-μ-diam metallic-coated spheres. The laser-optical system used to create the laser sheet in this study consists of a Lexel model 95A argon laser that produces a multimode laser beam in the range of 2–2.5 W, a series of optical lenses that focus the beam while maintaining its high intensity, and a rotating mirror, manufactured by Lincoln Laser Corporation. The rotating mirror is driven by a motor at 8.7 Hz to produce an effective scan frequency of 626 Hz. The focusing lenses and mirrors are located on a table that translates along the length of the water channel. The turning mirror and the rotating mirror are positioned on rails to allow translation of the laser sheet across the width of the channel and, therefore, adjustment of the plane of interest.

Multiple exposure images are taken of the flow field with a 105-mm lens mounted on a Nikon f4 (35-mm) camera, which records the displacements of particles over known time intervals. The magnification M of the lens is 0.2; this value is appropriate to obtain an overview of the larger scale features of the flow structure of interest in this experiment.

The camera looks into a bias mirror, which captures a reflection of the region of interest. The bias mirror oscillates in order to add a uniform velocity to all illuminated particles in the flow. This bias velocity overcomes negative velocities associated with regions of reverse flow and decreases the dynamic range of the particle images. Oscillation of the bias mirror and opening of the camera shutter are synchronized with the motion of the delta wing via the laboratory microcomputer.

The region of interest of the flowfield on each image lies below the delta wing (since a negative α was used in these experiments) and extends beyond the leading and trailing edges. This region covers a distance of $1.38c$, where c is the chord length in the plane of the image. All images were taken in a plane located $0.45\,c_0$ (7.62 cm) from the centerline of the delta wing, or approximately $2.1\,c_0$ (38.1 cm) from the channel wall. This plane is parallel to the centerline of the wing, as shown in Fig. 1. A schematic showing the location of a typical image relative to the delta wing is shown in the insets of Figs. 3–9. Further details are given by Cipolla.[7]

C. Interrogation Technique

The film negatives containing the patterns of particle images are interrogated, or analyzed, using a He-Ne laser to illuminate a 1.0-mm-diam area of the negative and produce an interference pattern. This pattern is transformed into Young's fringes via an optical Fourier transform. The fringe pattern is captured by a Cohu video camera and digitized in a 386 microcomputer. A second Fourier transform is performed on the digitized image allowing generation of the two-dimensional velocity vector corresponding to the illuminated region of the negative. The ratio of the interrogation step size to the magnification gives an effective grid size $\Delta\ell/M = d_I/2M = 2.5$ mm in the physical plane based on an interrogation spot size $d_I = 1.0$ mm, an interrogation overlap of 50% to satisfy the Nyquist criterion, and a lens magnification of 0.2. This interrogation grid size is 1.5% of the image width and between 3.1% and 3.8% of the image height.

Once a preliminary velocity field is obtained from the raw data, it is filtered to produce a complete, smooth field of velocity vectors. A constant Gaussian kernel of 1.3 is applied in this filtering process, the details of which are explained by Landreth and Adrian.[9] The filtered velocity field is then suitable for determining vorticity distributions and streamline patterns. The out-of-plane component of vorticity is computed numerically, and contours of constant vorticity are constructed via the program Surfer, which fits a spline curve through data points of equal vorticity values without additional filtering. A tension factor of 0.07 is specified for the spline curve fits. The sectional streamlines in the desired planes of flow are obtained by integrating the two-dimensional velocity data in that plane.

In all subsequent plots of vorticity and streamlines, the freestream flow is from left to right, positive vorticity (counter clockwise) is indicated by solid curves, and negative vorticity is indicated by dashed curves. The values of $\omega_{\min}$ and $\Delta\omega$ are both 0.0086 s^{-1} in the plane of the film, which correspond to a value of 5.4 s^{-1} in the physical flow plane, and are constant throughout this study to allow comparison of different regions of vorticity concentration. In the most concentrated vortex structures, the distance between consecutive vorticity contours corresponds to a minimum of one-fifth the interrogation grid size in the plane of the film, i.e., 0.1 mm.

III. Experiments and Interpretation of Results

A. General Experimental Conditions

The channel speed was maintained at a value of $U = 15$ cm/s, corresponding to a Reynolds number $Re_c \cong 22{,}000$ based on the root chord. To begin the experiment, the delta wing was set at the desired α, then allowed to oscillate through at least 20 cycles to ensure that the flowfield had reached a steady state before any pictures were taken. The dimensionless frequencies of oscillation of the wing were in the range $1.57 \leq k^* \leq 3.14$ in which

$$k^* = \pi f c_0 / U$$

where f is the forcing frequency, c_0 is the root chord, and U is the freestream velocity. The order of magnitude of k^* was guided by the study of Gursul et al.,[6] in which very high lift coefficients were obtained for an airfoil in an unsteady freestream oscillating at a reduced frequency near 1.0. This value was used as a starting point in the preliminary study. Since the oscillations induced by the wing are tangential, in contrast to the streamwise oscillations of Gursul et al.,[6] somewhat different values of k^* were found to be effective.

Three values of dimensionless wing oscillation frequency, $k^* = 1.57$, 2.09, and 3.14, were chosen for study at a nominal value of $\alpha = 30$ deg. One value, namely, $k^* = 3.14$, was also considered at nominal values of $\alpha = 35$ and 40 deg to show the dependence on angle of attack. The angular displacement $\Delta\alpha$ for all oscillations was ± 5 deg, corresponding to a displacement amplitude of the leading edge of the wing of approximately $0.09c_0$, where c_0 is the root chord.

Flowfield images were obtained as follows. The delta wing was initially set at the nominal angle of attack α, then oscillated at the desired value of k^*. Photographs were taken with the 35-mm camera over nine cycles of oscillation at the maximum, minimum, and nominal positions of each cycle. Also, images were acquired with the wing held stationary at each nominal α to allow comparison with the images obtained for the oscillating wing.

B. Instantaneous Flow Structure

1. Phase-Locked Response of the Flow Structure

The forcing conditions for which the flow structure on the wing is generally repetitive from one cycle to the next, i.e., phase locked

to the wing motion, are described by Cipolla.[7] Figure 3 shows a representative case corresponding to a nominal angle of attack $\alpha = 30$ deg and a dimensionless frequency $k^* = 1.57$. The instantaneous images correspond to the four positions A, B, C, and D during a typical cycle of oscillation; also shown are images for the stationary wing at $\alpha = 30$ deg.

First, note the existence of the large, coherent vortex structure in image B, when the wing has reached its maximum amplitude of the oscillation, in contrast to the large region of separated, reverse flow indicated in the vorticity contours and the streamline patterns on the stationary wing. In image B, the vorticity layer from the leading edge evolves into a large-scale leading-edge vortex located close to the surface of the wing. At later instants, shown in images C and D, the vortex moves downstream and eventually reappears at the same position B in the next cycle of oscillation. Also, note that the initial region of the vorticity layer formed in image B actually consists of several smaller, discrete concentrations of vorticity. This observation is analogous to the dye visualization of Gad-el-Hak and Blackwelder[10]; small-scale vortices shed from the leading edge of a delta wing at constant angle of attack merge to form the large-scale, leading-edge vortex. These discrete vortices can be identified as Kelvin–Helmholtz instabilities having their origin in the linearly unstable shear layer, as described by Monkewitz and Heurre.[11] Other authors have observed discrete vortices in free shear layers originating from a splitter plate between streams of different velocities, for example, and noted a similar pairing process which creates a single, larger vortex.[10]

In image B, the streamline pattern corresponding to the large-scale vortex exhibits the form of an outward spiral. According to critical point theory, this type of structure corresponds to an unstable focus.[12] Image C shows that the inner portion of the vortex has transformed to an inward spiral, i.e., a stable focus. The transition from an unstable to a stable focus results in a limit cycle appearing in the streamline pattern of image C. This observation is analogous to the topology observed by Visbal[13] in his numerical study of the transient relaxation of the leading-edge vortex on a delta wing. Finally, in image D, the structure has evolved into a completely stable focus, as represented by the inwardly spiraling streamlines. It is evident that the structure of the leading-edge vortex rapidly transforms through a succession of states as it develops and moves downstream. It is not possible, however, to deduce conclusively whether the leading-edge vortex is undergoing compression or extension; additional orientations of the plane of observation are required.[13]

Also of interest is the tendency of the streamlines to intersect in the lower middle portions of images A and B of Fig. 3. This intersection corresponds to a saddle point in critical point theory. During the subsequent stage of development of the leading-edge vortex, shown in images C, this saddle point vanishes in favor of a nodal

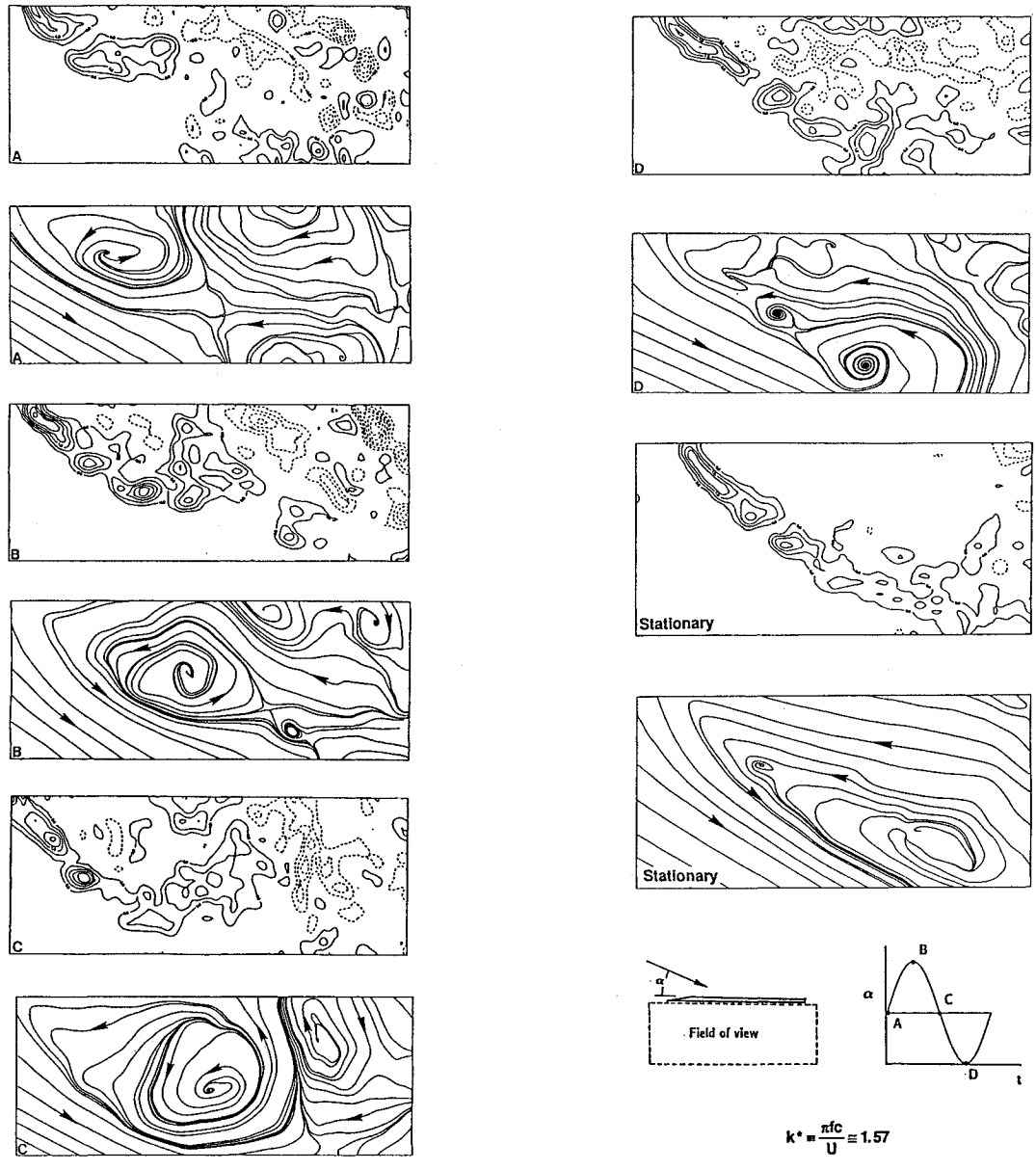

Fig. 3 Instantaneous vorticity contours and streamline patterns for phase-locked response of flow structure; $\alpha = 30$ deg, $\Delta\alpha = \pm 5$ deg, $\omega_{min} = \Delta\omega = 5.4\ s^{-1}$.

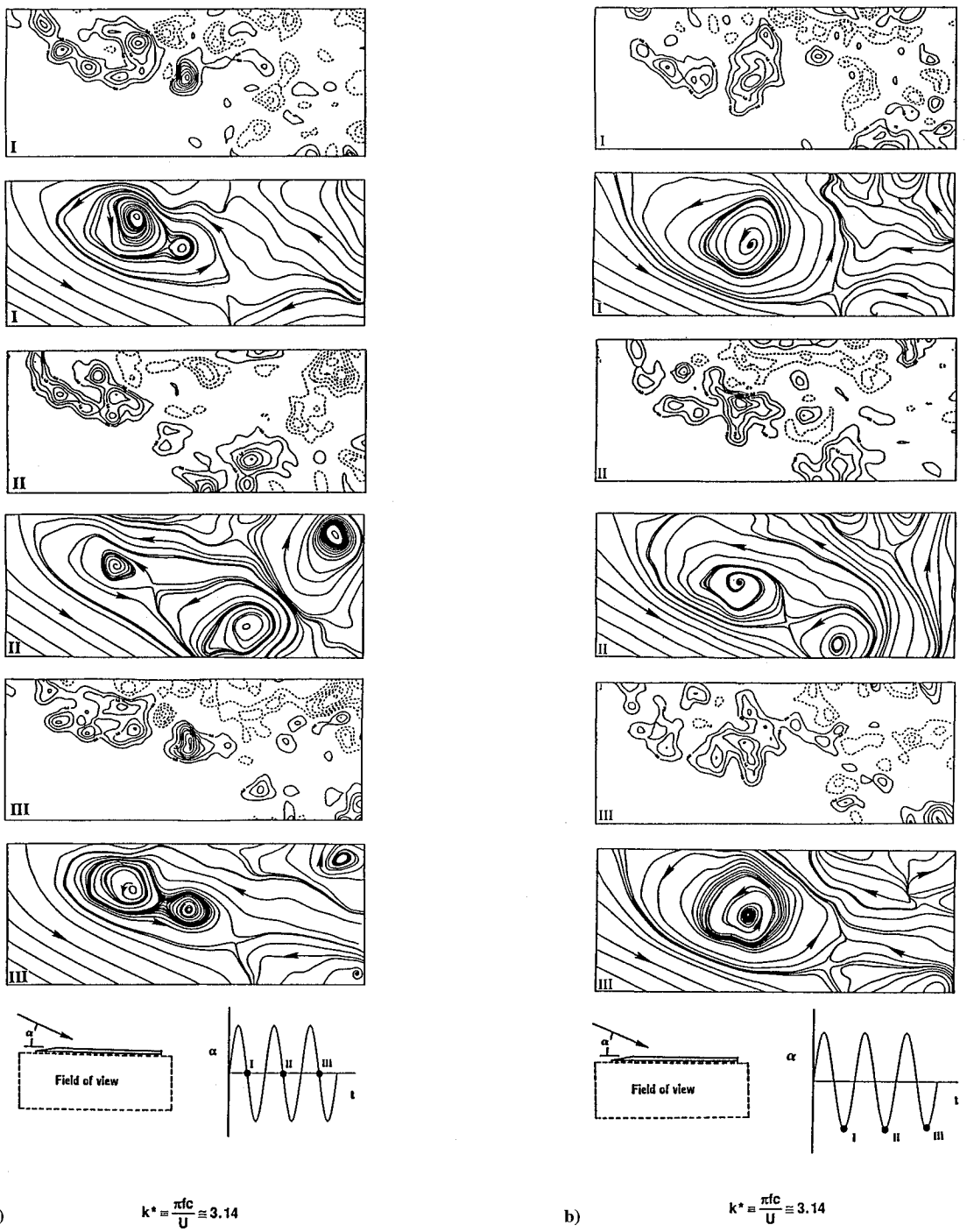

Fig. 4 Instantaneous vorticity contours and streamline patterns for subharmonic response of flow structure; α = 30 deg, $\Delta\alpha = \pm 5$ deg, $\omega_{min} = \Delta\omega = 5.4\ s^{-1}$; images taken at a) nominal α during downstroke and b) minimum angle of attack.

line, characterized by the coalescence of several streamlines. Comparison with the corresponding vorticity pattern of image C suggests that this nodal line represents the boundary between the large-scale, (positive vorticity) leading-edge vortex and a large vortical structure of negative vorticity located in the vicinity of, and apparently emanating from, the trailing edge. Subsequently, as exhibited in the vorticity pattern of image D, the cluster of negative vorticity moves upstream. Such negative vorticity is not present in the image corresponding to the stationary wing. It, therefore, may be concluded that the oscillating motion of the trailing edge serves as a source of negative vorticity that coexists with the positive vorticity formed from the leading edge.

2. Nonphase-Locked (Subharmonic) Response of the Flow Structure

At sufficiently high reduced frequency k^*, the flow structure repeats every other cycle of the wing motion, i.e., at the subharmonic of the forcing frequency.[7] Figure 4a shows images from three consecutive cycles at a dimensionless frequency $k^* = 3.14$. Each set of images represents the same delta wing position during the oscillation cycle. It is apparent that the patterns approximately repeat every other cycle of the wing motion. Note the correlation between images I and III, which occur two periods apart. Two strong concentrations of vorticity are clearly seen in both images. Image II, however, shows a markedly different pattern, which includes a strong negative vorticity concentration at the trailing edge but lacks the strong vorticity concentration present in the center of images I and III. The accompanying streamline patterns corroborate these observations.[7]

This subharmonic response is illustrated further in Fig. 4b, for the minimum angle of attack of the wing during oscillation. Once again, images I and III show very similar patterns, whereas the pattern of image II is distinctly different. Images I and III contain

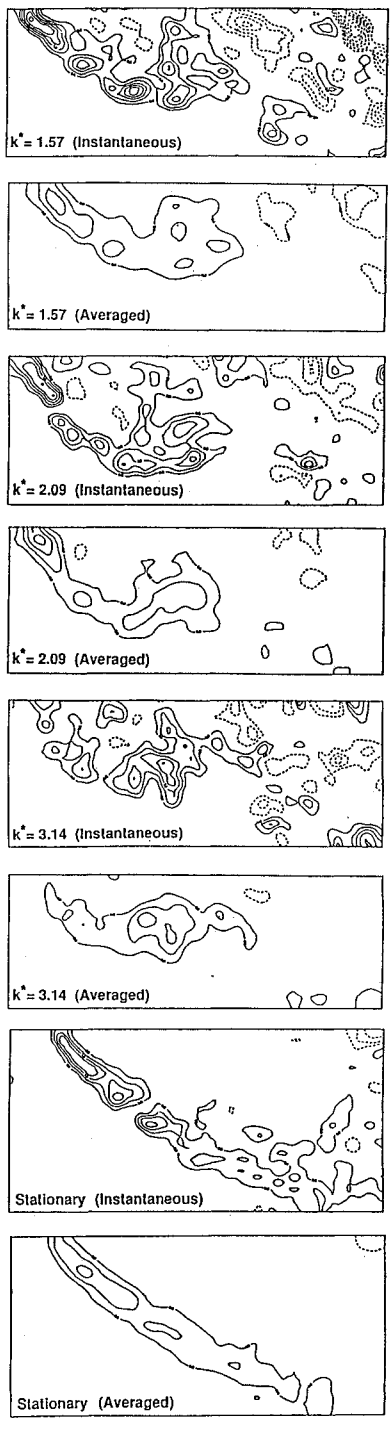

Fig. 5 Instantaneous vs ensemble-averaged vorticity contours; α = 30 deg, $\Delta\alpha = \pm 5$ deg, $\omega_{min} = \Delta\omega = 5.4\ s^{-1}$.

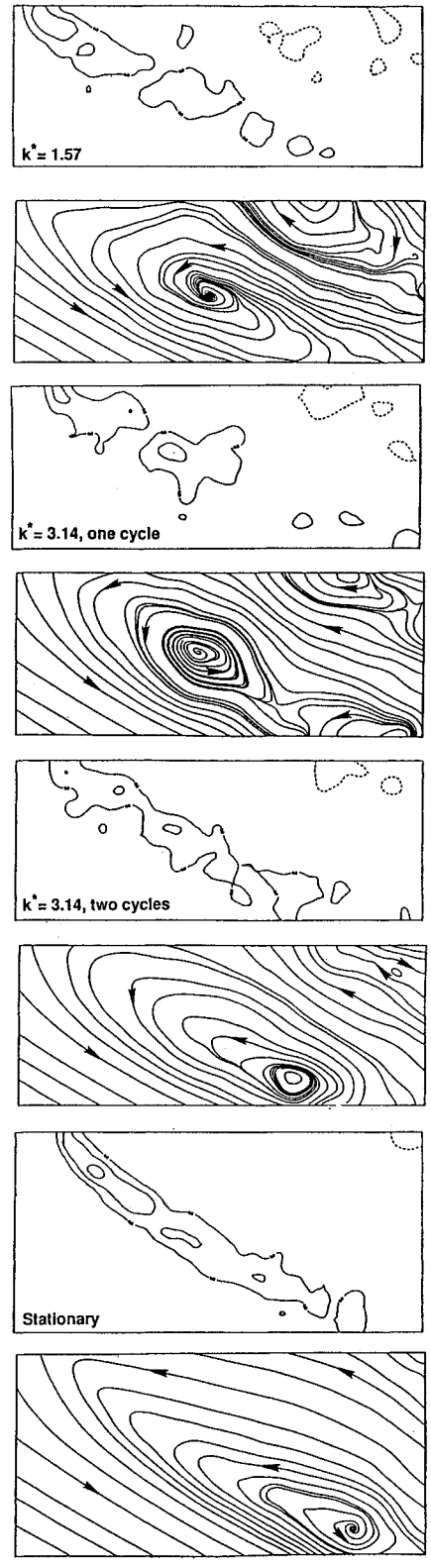

Fig. 6 Cycle-averaged structure, α = 30 deg, $\Delta\alpha = \pm 5$ deg, $\omega_{min} = \Delta\omega = 5.4\ s^{-1}$.

a large-scale coherent vortex close to the wing surface. The single spiral pattern in these images disappears in favor of two smaller spiral patterns in image II, which correspond to two concentrations of vorticity.

Several critical point patterns are evident in the streamline patterns of Figs. 4a and 4b. In each of the streamline patterns of images I–III in Fig. 4a there is a saddle point (intersection of streamlines) between the two adjacent vortices; moreover, downstream of this pair of vortices in images I and III, there is an additional saddle point. A saddle point also consistently develops in the lower right portions of images I and III in Fig. 4b. However, in image II of Figs. 4a and 4b, a saddle point occurs between the two pronounced vortices only; none is seen downstream of them. Considering together all of the images of Figs. 4a and 4b, it is evident that not only the number and location of centers of vortex-spiral streamlines (foci), but also the position and number of saddle points, provide a means of identifying the alternating flow patterns associated with the subharmonic response of the flow structure.

C. Instantaneous vs Ensemble-Averaged Flow Structure

Figure 5 compares representative instantaneous vorticity distributions with their corresponding ensemble-averaged distributions. In each case, the averaged image was determined from the velocity fields of four instantaneous images obtained at the same phase of the oscillation cycle of the wing. Although the same general patterns exist in the averaged and instantaneous plots, considerably lower

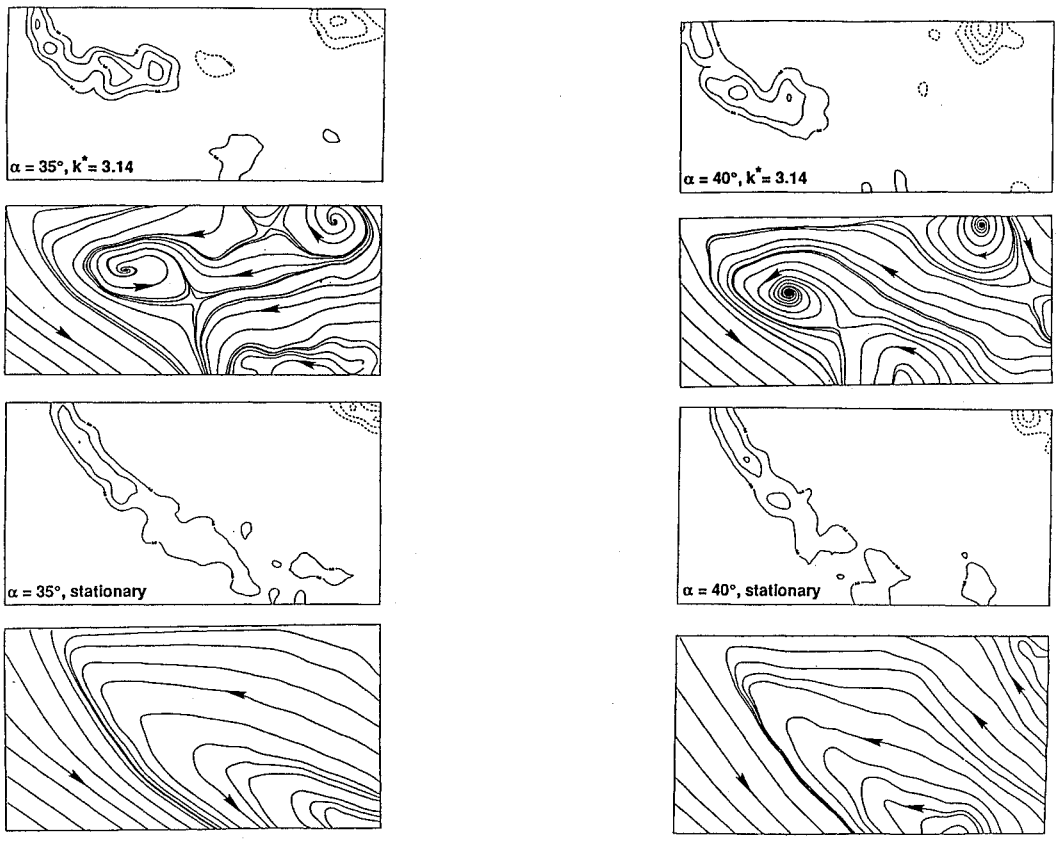

Fig. 7 Ensemble-averaged structure, α = 35 deg and α = 40 deg, $\omega_{min} = \Delta\omega = 5.4\ s^{-1}$.

levels of vorticity are seen in the averaged contours. Evidently, the locations of the small-scale vortices initially formed in the shear layer from the leading edge are not phase locked with the wing motion. In contrast, the large-scale vortices appear in both the instantaneous and averaged contour plots, indicating that their formation is generally phase locked. This observation suggests that the phase-repeated formation of large-scale vortices close to the wing may produce enhanced, phase- (ensemble-) averaged lift. Elimination of some vorticity levels also is seen when comparing the instantaneous and averaged contours for the stationary wing, although the effect is less dramatic. This dramatic attenuation of the peak vorticity levels of the small-scale structures due to limited ensemble-averaging suggests that such vortical structures would not be detected when successive point measurements are taken in the traditional sense with a single probe.

D. Cycle-Averaged Flow Structure

The four images constituting a complete oscillation cycle were averaged to determine the dominant, averaged structure over the entire cycle. The vorticity contours and streamlines for three representative cases are shown in Fig. 6. Note that two sets of images are shown for $k^* = 3.14$. One set corresponds to the average of the four images from a single cycle containing the pronounced vortical structure seen in images I and III in Fig. 4b; the other corresponds to the average of eight images from two consecutive cycles at $k^* = 3.14$.

Note that, after cycle averaging, the form of the vorticity contours for the cycle averages at $k^* = 1.57$ and 3.14 approaches that of the stationary, or stalled, wing. This observation suggests that the cycle-averaged lift is unlikely to depart significantly from that of the stationary wing. Also, as demonstrated via the results of Sec. III.C, the averaging process eliminates most of the small-scale vortices and lowers the vorticity levels overall.

The existence of a fairly coherent vortex structure in the vorticity contour plot corresponding to the average of one cycle at $k^* = 3.14$ suggests that the large-scale vortex seen in images I and III in Fig. 4b is prevalent throughout the entire cycle. However, when the average of two consecutive cycles is considered, this structure is lost, indicating that a coherent vortex is formed close to the wing surface only during every other cycle of the wing motion. The locations of foci (vortex centers) in the streamline patterns of Fig. 6 can be used to compare the cycle-averaged flow structures with those of the stationary wing. Note that in the images corresponding to $k^* = 1.57$ and the single-cycle average for $k^* = 3.14$, the foci are located closer to the wing surface than for the case of the stationary wing. In contrast, the streamline pattern for the two-cycle-averaged case is almost identical to that on the stationary wing, with the focus located substantially downstream of the wing. Again, the resemblance of the cycle-averaged vorticity and streamline patterns to those of the stalled wing demonstrates the effects of the averaging process.

E. Effect of Angle of Attack on Flow Structure

Following the procedure used in previous experiments, the delta wing was set at a nominal $\alpha = 35$ or 40 deg, compared to $\alpha = 30$ deg in the preceding cases, and forced to oscillate at a dimensionless frequency $k^* = 3.14$. Figure 7 compares averaged contours of constant vorticity and streamline patterns for the oscillating wing to the averaged patterns for a stationary wing at the same angle of attack. Each averaged image was obtained by ensemble averaging four phase-referenced instantaneous velocity fields. The images shown for the oscillating wing correspond to the wing passing through its nominal α (denoted as point C in the inset of Fig. 3). Inspection of the vorticity contours for the oscillating wing at nominal angles of attack equal to 35 and 40 deg shows formation of an identifiable vortex, in contrast to the case of the stationary wing. In summary, oscillating motion of the wing decreases the extent of the stall region and promotes formation of a leading-edge vortex in a manner similar to that observed at the lower angle of attack. However, these effects are less dramatic at these higher angles of attack, $\alpha = 35$ and 40 deg, than at $\alpha = 30$ deg.

IV. Conclusions

Harmonic oscillation of a delta wing at high angle of attack can decrease substantially the extent of the stall region. This is evidenced by roll up of the vorticity layer from the leading edge into a large-scale vortex structure close to the wing surface during part of the oscillation cycle. Recurrence of this large-scale structure over

successive cycles of oscillation suggests a corresponding increase in phase-averaged lift. The particular flow structure produced by oscillation of the wing and the degree of repeatability depend on the dimensionless oscillation frequency k^*.

Two basic, highly repeatable modes of response of the flow structure were observed. The first involves repetitive patterns of large-scale vortex formation locked in to the wing motion at the forcing frequency. The second mode involves repetitive patterns every other cycle of the wing motion, i.e., at the subharmonic of the forcing frequency. The advantage of the subharmonic response is that the time-(cycle-) averaged flow structure shows a more coherent leading-edge vortex relative to that of the locked-in or the stationary cases.

Patterns of instantaneous sectional streamlines over a cross section of the leading-edge vortex exhibit various flowfield topologies. Such topology, involving several types of critical points at defined locations, can allow identification of the physical processes in the flowfield and the classes of vortex formation.

Traditional ensemble-averaging techniques are compared with phase-referenced patterns of instantaneous velocity fields. Small-scale vortical structures in the flow that are not repeatable from cycle to cycle are averaged out, and the overall vorticity levels are substantially lowered relative to the true, instantaneous values.

Acknowledgment

The financial support of the Air Force Office of Scientific Research under AFOSR Grant F49620-92-J-0328 is gratefully acknowledged.

References

[1]Gad-el-Hak, M., "Unsteady Separation on Lifting Surfaces," *Applied Mechanics Review*, Vol. 40, April 1987, pp. 441–453.

[2]Magness, C., Robinson, O., and Rockwell, D., "Control of Leading-Edge Vortices on a Delta Wing," AIAA Paper 89-0999, March 1989.

[3]Lee, M., and Ho, C. M., "Lift Force of Delta Wings," *Applied Mechanical Review*, Vol. 43, Sept. 1990, pp. 209–220.

[4]Ashley, H., Katz, J., Jarrah, M., and Vaneck, T., "Survey of Research on Unsteady Aerodynamic Loading of Delta Wings," *Journal of Fluids and Structures*, Vol. 5, 1991, pp. 363–390.

[5]Rockwell, D., "Three-Dimensional Flow Structure on Delta Wings at High Angle-of Attack: Experimental Concepts and Issues," AIAA Paper 93-0550, Jan. 1993.

[6]Gursul, I., Lin, H., and Ho, C. M., "Vorticity Dynamics of 2-D and 3-D Wings in Unsteady Free Stream," AIAA Paper 91-0010, Jan. 1991.

[7]Cipolla, K., "Control of Leading-Edge Vortices on a Harmonically Oscillating Delta Wing," M.S. Thesis, Dept. of Mechanical Engineering and Mechanics, Lehigh Univ., Bethlehem, PA, Nov. 1992.

[8]Rockwell, D., Magness, C., Towfighi, J., Akin, O., and Corcoran, T., "High Image-Density Particle Image Velocimetry Using Laser Scanning Techniques," *Experiments in Fluids*, Vol. 14, 1993, pp. 181–192.

[9]Landreth, C. C., and Adrian, R. J., "Measurement and Refinement of Velocity Data Using High Image Density Analysis in Particle Image Velocimetry," *Applications of Laser Anemometry to Fluid Mechanics: Proceedings of the 4th International Symposium*, edited by R. J. Adrian, T. Asanuma, D. Durão, F. Durst, and J. Whitlaw, Springer–Verlag, Berlin, 1988, pp. 484–497.

[10]Gad-el-Hak, M., and Blackwelder, R. F., "The Discrete Vortices from a Delta Wing," *AIAA Journal*, Vol. 23, No. 6, 1985, pp. 961, 962.

[11]Monkewitz, P. A., and Heurre, P., "Influence of the Velocity Ratio on the Spatial Stability of Mixing Layers," *Physics of Fluids*, Vol. 25, No. 7, 1982, pp. 1137–1143.

[12]Perry, A. E., and Steiner, T. R., "Large-Scale Structures Vortex in Turbulent Wakes Behind Bluff Bodies. Part 1. Vortex Formation Processes," *Journal of Fluid Mechanics*, Vol. 174, 1987, pp. 233–270.

[13]Visbal, M. R., "Structure of Vortex Breakdown on a Pitching Delta Wing," AIAA Paper 93-0434, Jan. 1993.